The Higgs signatures at the CEPC CDR baseline*

Hang Zhao(赵航)[1,2,3] Yong-Feng Zhu(朱永峰)[1,4] Cheng-Dong Fu(傅成栋)[1]
Dan Yu(于丹)[1] Man-Qi Ruan(阮曼奇)[1,2;1)]

[1]Institute of High Energy Physics, Chinese Academy of Sciences, Beijing 100049, China
[2]CAS Center for Excellence in Particle Physics, Beijing 100049, China
[3]Collaborative Innovation Center for Particles and Interactions, Hefei 230026, China
[4]University of Chinese Academy of Sciences, Beijing 100049, China

Abstract: As a Higgs factory, the CEPC (Circular Electron-Positron Collider) project aims at precision measurements of the Higgs boson properties. A baseline detector concept, APODIS (A PFA Oriented Detector for the HIggS factory), has been proposed for the CEPC CDR (Conceptual Design Report) study. We explore the Higgs signatures for this baseline design with $\nu\bar{\nu}$ Higgs events. The detector performance for reconstructing charged particles, photons and jets is quantified with $H \to \mu\mu, \gamma\gamma$ and jet final states, respectively. The resolutions of reconstructed Higgs boson mass are comparable for the different decay modes with jets in the final states. We also analyze the $H \to WW^*$ and ZZ^* decay modes, where a clear separation between different decay cascades is observed.

Keywords: CEPC, Higgs boson, full simulation

PACS: 13.66.Fg, 13.66.Jn, 14.80.Bn **DOI:** 10.1088/1674-1137/43/2/023001

1 Introduction

After the Higgs boson discovery [1,2] at the LHC (Large Hadron Collider), precision measurements of the Higgs boson properties are of particular importance. The CEPC, a future high energy collider project based on a 100 km circumference main ring [3], is therefore proposed. Operating at 240 GeV center-of-mass energy, the CEPC is designed for an instantaneous luminosity of $\sim 3\times10^{34}\mathrm{cm}^{-2}\mathrm{s}^{-1}$ and could deliver 10^6 Higgs bosons (5 ab^{-1} integrated luminosity) in about 10 years [4]. The absolute Higgs boson couplings can be measured to a relative accuracy of 0.1% - 1% at the CEPC, roughly one order of magnitude superior to the Higgs signal strength at the HL-LHC [5,6].

At the CEPC, the Standard Model (SM) Higgs bosons are produced mainly through the Higgsstrahlung process ($e^+e^- \to ZH$) , the vector boson fusion processes (the Z fusion process $e^+e^- \to e^+e^-H$, and the W fusion process $e^+e^- \to \nu\bar{\nu}H$), see Fig. 1. The corresponding cross sections with the 125 GeV SM Higgs boson using non-polarized beam at different center-of-mass energies are shown in Fig. 2 [7]. At the CEPC, roughly a quarter of the Higgs bosons are produced in association with a pair of neutrinos ($\nu\bar{\nu}H$), including both the W fusion events and the ZH events with Z decays to $\nu\bar{\nu}$. The Higgs decay products are responsible for almost all the detector signals of these $\nu\bar{\nu}H$ events, providing benchmark samples for the CEPC detector performance study.

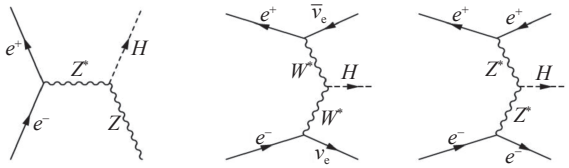

Fig. 1. Feynman diagrams of the Higgs production mechanisms at the CEPC: the Higgsstrahlung, WW fusion, and ZZ fusion processes.

This paper presents a performance analysis of the CEPC baseline detector geometry APODIS (also known as the CEPC_v4) [8]. Using fully simulated $\nu\bar{\nu}H$ samples, we analyze a set of Higgs distributions that cover all the major SM Higgs decay modes. In Section 2, we intro-

Received 13 July 2018, Revised 29 October 2018, Published online

* Supported by National Key Program for *S&T* Research and Development (2016YFA0400400), the National Natural Science Foundation of China (11675202), and the Hundred Talent programs of Chinese Academy of Science (Y3515540U1)

1) E-mail: manqi.ruan@mail.ihep.ac.cn

duce the baseline detector and the software tools. Section 3 discusses the reconstruction results of the Higgs signals. A conclusion is given in Section 4.

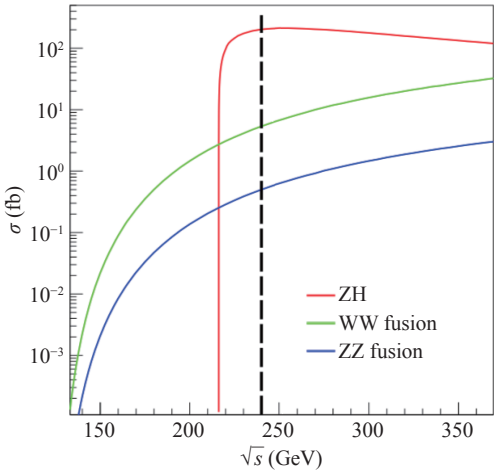

Fig. 2. (color online) Production cross sections of the Higgsstrahlung, *WW* fusion and *ZZ* fusion processes as function of center-of-mass energy, shown as colored lines. The dashed line (black) refers to the possible operating energy of the CEPC ($\sqrt{s}$ = 240 GeV) .

2 Baseline detector and CEPC software chain

APODIS (CEPC_v4), is optimized from the CEPC_v1 conceptual detector, which is the reference detector design for the CEPC Preliminary Conceptual Design Report (CEPC PreCDR, published in 2015) [3]. Both conceptual detectors consist of a silicon pixel vertex detector, a tracking system composed of a time projection chamber (TPC) and several silicon detectors, and a high granularity calorimetry system including an electromagnetic calorimeter and a hadronic calorimeter. More information on the geometry of CEPC_v1 can be found in Ref. [3], and the performance study results can be found in Ref. [9]. Compared to CEPC_v1, APODIS maintains the same level of performance for Higgs signals (lepton identification and reconstruction of photon and jets). As a result of a series of optimization studies, the number of calorimeter readout channels, the total weight and the solenoid B-field of APODIS have been significantly reduced. The ECAL transverse cell size is now enlarged, from 5 mm by 5 mm to 10 mm by 10 mm [10]. The HCAL is shorter, 40 layers instead of 48 layers [11]. The solenoid B-field is reduced from 3.5 T to 3 T due to the requirements of the MDI design [12]. A time-of-flight (ToF) detector is proposed which significantly enhances the performance for the charged Kaon identification [13]. More information on the geometry and simulation results can be found in Ref. [8].

A complete simulation-reconstruction toolkit has been established and optimized for the APODIS geometry. The information flow consists of three basic modules: Generation, Simulation, and Reconstruction. For Generation, Whizard [15] and Pythia [16] are used to generate final state particles for physics processes. The samples are then fully simulated using the Geant4 based simulation framework MokkaPlus [17, 18], and reconstructed using Arbor [19] for the core Particle Flow [20] reconstruction. Figure 3 shows the information flow and major processes of the software chain.

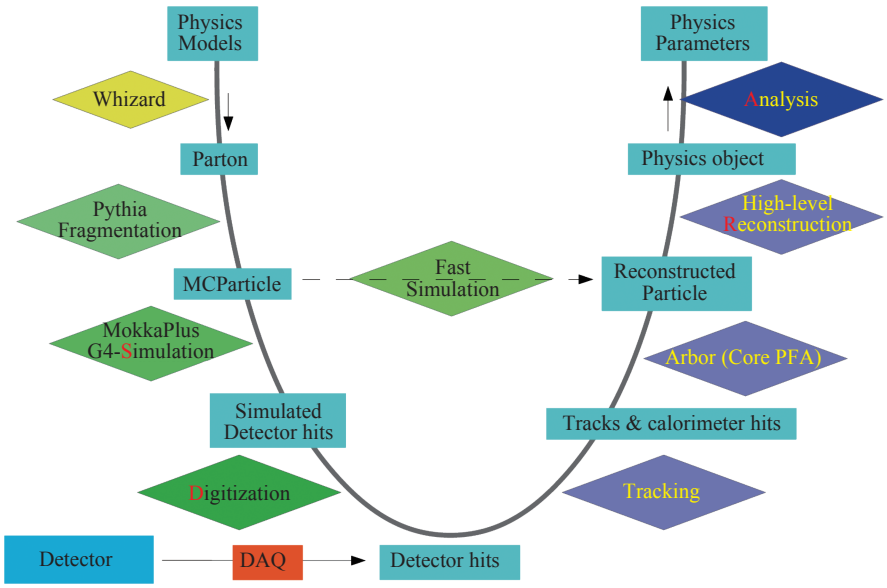

Fig. 3. (color online) Information flow and major processes of the CEPC software chain. For Generation, Whizard and Pythia are used to generate final state particles for physics processes. MokkaPlus is used for Simulation. The simulated detector hits are digitized and then used by reconstruction algorithms to get physics objects, which are further analyzed for physics parameters.

3 Benchmark distributions of the Higgs signals using $\nu\bar{\nu}H$ events

We simulate and reconstruct the $\nu\bar{\nu}H$, $H \to \gamma\gamma$, $\mu\mu$, gg, bb, cc, WW*, ZZ* samples, each with ~50000 events. Most of the Standard Model Higgs boson decay modes are included except $H \to \tau\tau$, which was extensively studied in Ref [11]. For the $H\to\gamma\gamma$ and $H\to\mu\mu$ events, the decay products can be directly identified from the reconstructed particles, and the reconstruction performance is related to the performance of the tracking system or the ECAL. For the other decay events ($H \to bb$, cc, gg, WW*, ZZ*), we compute the total invariant mass of the events using all reconstructed particles. In these fully reconstructed events, the total invariant mass distributions are not only related to the detector performance but are also affected by other physics effects, notably:

- The ISR (initial state radiation) photons.
- The neutrinos generated by the Higgs boson decay products.
- The direction of jets from Higgs to a pair of jet events, due to the acceptance of the detector.

Figure 4 shows the correlation between the computed Higgs boson mass using all reconstructed particles and these effects, for the $H \to gg$ events. The calculation of these effects is based on Monte Carlo truth information. $Pt_{\rm ISR}$ is calculated by summing the transverse momentum of all ISR photons. $Pt_{\rm neutrino}$ is the sum of the transverse momentum of the neutrinos generated by Higgs boson decay products. $|\cos\theta_{\rm Jet}|$ is the minimum angle between the beam pipe and the quarks generated by the Higgs boson. Clearly, a strong correlation is observed when these effects are significant. In order to disentangle these effects from the detector performance at jet reconstruction, Monte Carlo truth level event selection is applied to the events with jets in the final states. The cleaning procedure is set up using $Pt_{\rm ISR} < 1$ GeV, $Pt_{\rm neutrino} < 1$ GeV and $|\cos\theta_{\rm Jet}| < 0.85$, with selection efficiencies shown in Table 1. The cut values used for event cleaning are shown with red lines in Fig. 4.

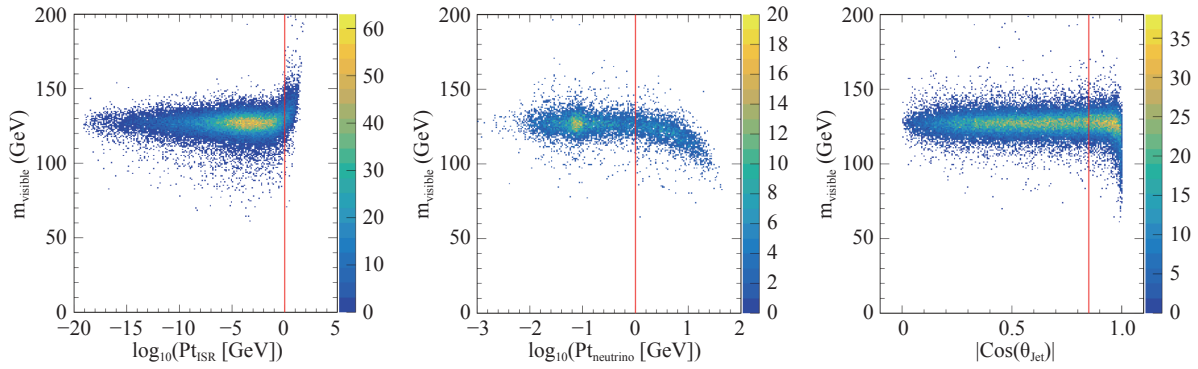

Fig. 4. (color online) Correlation between the reconstructed Higgs boson mass and the sum of the transverse momentum of the ISR photons ($Pt_{\rm ISR}$) (left); the sum of the transverse momentum of the neutrinos generated by the Higgs bosons decay products ($Pt_{\rm neutrino}$) (center); and the minimum angle between jets and the beam pipe ($|\cos\theta_{\rm Jet}|$) (right). These plots are based on the $H \to gg$ events, and similar conclusions are obtained with $H \to bb$ and cc events. The red lines in the plots are the cut values used for event cleaning.

Table 1. Event cumulative efficiency for Higgs boson exclusive decay at the CEPC with $\sqrt{s} = 240$ GeV.

	gg(%)	bb(%)	cc(%)	WW*(%)	ZZ* (%)
Pt_ISR < 1 GeV	95.15	95.37	95.30	95.16	95.24
Pt_neutrino < 1 GeV	89.33	39.04	66.36	37.46	41.39
|Cos(Theta_Jet)| < 0.85	67.30	28.65	49.31	–	–

3.1 $H\to\mu\mu$

The Higgs boson decay into $\mu^+\mu^-$ is a rare process with a branching ratio of 0.022% for the 125 GeV SM Higgs boson [21]. From the reconstructed particles, we select a pair of muons with opposite charge and with energies greater than 20 GeV. The invariant mass of this pair of muons is reconstructed as the Higgs boson mass. The distribution fitted by a Crystal Ball function [22, 23] is shown in Fig. 5. The long tail on the left of the peak is induced by the radiation effects (ISR, FSR, bremsstrahlung, etc), while the beamstrahlung effect is negligible in the CEPC. The tracking performance is characterized by the sigma/mean of the fitted results, which is 0.20% for this benchmark channel.

3.2 $H\to\gamma\gamma$

The performance of the ECAL (electromagnetic calorimeter) is characterized by the reconstruction of the $H\to\gamma\gamma$ events. We select two most energetic photons

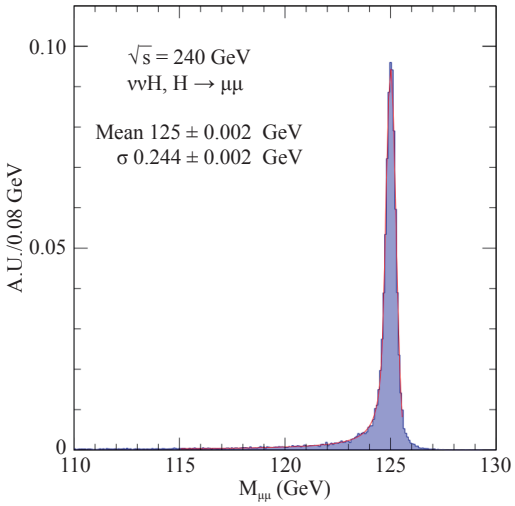

Fig. 5. (color online) Distribution of the reconstructed Higgs boson mass for $H \to \mu\mu$ events fitted by a Crystal Ball function.

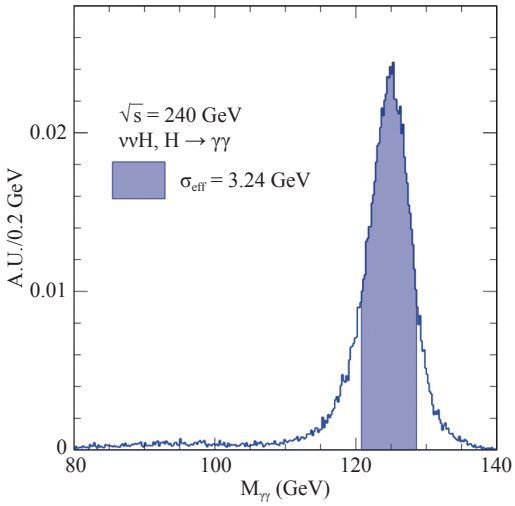

Fig. 6. (color online) Distribution of the reconstructed Higgs boson mass for $H \to \gamma\gamma$ events, parametrized with the half-width of the narrowest interval containing 68.3% of the distribution ($\sigma_{\rm eff}$). The mean value of the interval events is calibrated to 125 GeV.

with energies higher than 10 GeV and calculate their invariant mass, see Fig. 6. The tail on the left is caused by the geometry defects and the material upstream of the calorimeter. The width of the distribution is parametrized by the half-width of the narrowest interval containing 68.3% of the distribution, $\sigma_{\rm eff}$ [24]. The mean value of the interval events has been calibrated to 125 GeV. The $\sigma_{\rm eff}$ of the distribution is 3.24 GeV and the resolution (sigma/mean) is 2.59%. The resolution is limited by the absence of adequate geometry-based corrections and fine-tuned calibrations. The reconstructed Higgs boson mass resolution is 1.64% when using a simplified electromagnetic calorimeter geometry [10]. This simplified geometry has no geometry defects and no materials before ECAL, and uses similar ECAL geometry parameters as APODIS. Compared to the resolution with the simplified geometry, APODIS is 58% worse. Further geometry-based corrections and calibrations are under development.

3.3 $H \to bb, cc, gg$

Roughly 70% of the 125 GeV SM Higgs bosons decay into a pair of jets (bb, cc, and gg). For these events, we collect all the reconstructed particles and calculate their invariant mass. The distributions of reconstructed Higgs boson mass before event selection are shown in Fig. 7. Figure 8 shows the results after applying the event selection described above. After cleaning, the resolutions of Higgs boson mass for different decay channels of Higgs to a pair of jets are almost identical, 3.63% (bb), 3.82% (cc) and 3.75% (gg). These resolutions can be used to characterize the performance for jet reconstruction.

3.4 $H \to WW^*$

The 125 GeV SM Higgs boson has a probability of 21.4% to decay into a pair of W bosons. Limited by the Higgs boson mass, one of the W boson is off-shell (W^*). The reconstructed total visible invariant mass distribution is shown in Fig. 9. Depending on the decay modes of W and W^* (leptonic or hadronic), the total invariant mass

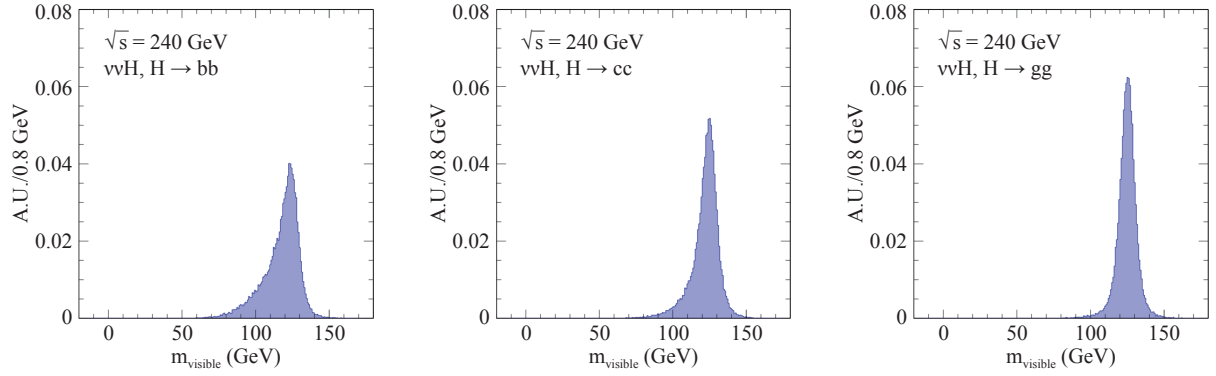

Fig. 7. (color online) Distributions of the reconstructed total visible invariant mass for $H \to bb, cc, gg$ events before event cleaning.

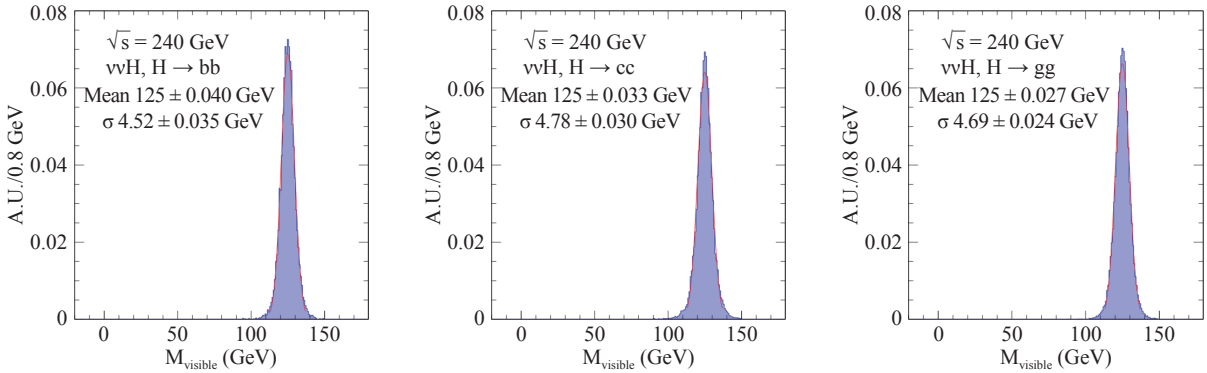

Fig. 8. (color online) Distributions of the reconstructed total visible invariant mass for $H \to bb, cc, gg$ events after event cleaning and fitted by Gaussian functions. The resolutions (sigma/mean) of the fitted results are 3.63% (bb), 3.82% (cc), and 3.75% (gg).

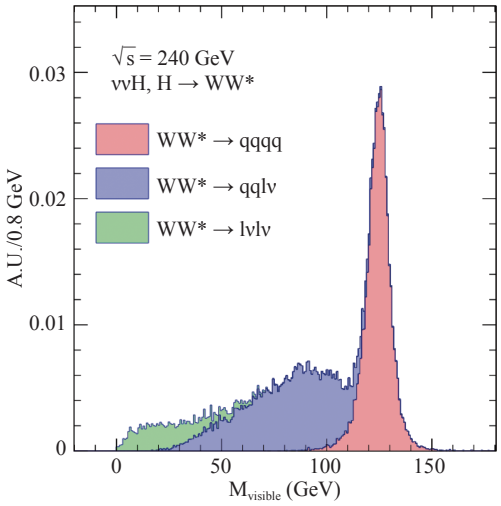

Fig. 9. (color online) Cumulative distribution of reconstructed total visible invariant mass for $H \to WW^*$ events. Depending on the decay modes of W and W^* ($WW^* \to qqqq$, $WW^* \to qql\nu$ and $WW^* \to l\nu l\nu$), the total invariant mass distribution is decomposed into three sub-distributions.

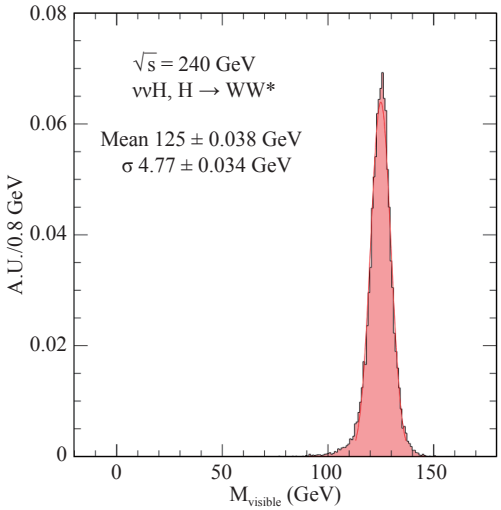

Fig. 10. (color online) Distribution of reconstructed total visible invariant mass for $H \to WW^*$ events after event cleaning, fitted by a Gaussian function. These events are selected from $WW^* \to qqqq$ events.

distribution is decomposed into different sub-distributions. The main peak at 125 GeV corresponds to events where both W and W^* decay into two quarks. The other two signals correspond to events where W or W^* decay into a lepton and a neutrino.

The event selection procedure is also applied. After event cleaning, the events for which W or W^* decay into leptons and neutrinos are excluded, as shown in Fig. 10. The cleaned invariant mass distribution is fitted by a Gaussian function with a σ=4.77 GeV. The fit result is comparable with the Higgs decay into two jet events.

3.5 $H \to ZZ$

About 2.6% of the 125 GeV SM Higgs bosons decay into ZZ^*. Similar to the $H \to WW^*$ channel, one of the Z bosons is off-shell. The Z bosons then decay into $q\bar{q}$ (~70%), $l\bar{l}$ (~10%) or $\nu\bar{\nu}$ (~20%).

Figure 11 shows the reconstructed total invariant mass. With Monte Carlo truth information, the events are classified depending on the decay modes of Z and Z^* (visible or invisible). There are four peaks in the distribution. The peak at zero invariant mass corresponds to the events where both Z and Z^* decay into neutrinos, which is about 4% of all events. The main peak at the expected Higgs boson mass (~125 GeV) corresponds to events where all final state particles are visible. The other two peaks correspond to conjugate cases where $Z \to$ visible , $Z^* \to$ invisible and $Z^* \to$ visible , $Z \to$ invisible

When event selection procedure is used, the events where Z or Z^* decay into neutrinos are excluded, as shown in Fig. 12. Depending on the Z decay modes, most of the remaining events contain 2 or 4 quarks as final state particles. The cleaned invariant mass distribution is fitted by a Gaussian function with a σ=4.68 GeV. The resolution is also comparable with the Higgs decay into two jet events.

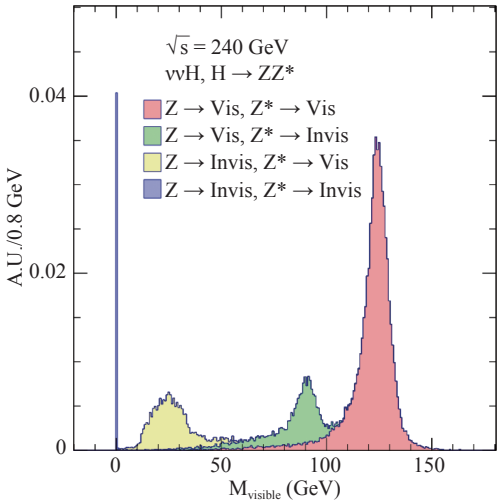

Fig. 11. (color online) Cumulative distribution of reconstructed total invariant mass for $H \to ZZ^*$ events, classified by the decay modes of Z and Z^* (visible or invisible).

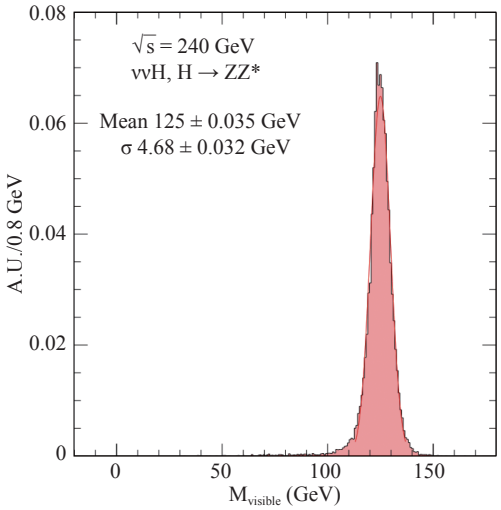

Fig. 12. (color online) Distribution of reconstructed total visible invariant mass for $H \to ZZ^*$ events after event selection, fitted by a Gaussian function. In these events, both Z and Z^* decay to visible products.

4 Conclusion

Based on the APODIS detector design, we characterize the Higgs signatures for $e^+e^- \to \nu\bar{\nu}H$ events with Higgs decays into $\gamma\gamma$, $\mu\mu$, gg, bb, cc, WW^* and ZZ^*. With the Higgs to $\mu\mu$, $\gamma\gamma$ and jet final state events, we assess the detector performance by quantifying the resolution of the Higgs invariant mass for various channels, as shown in Table 2. Compared to the corresponding resolutions at the LHC, the resolution for $H \to \mu\mu$ events is one magnitude superior. For the Higgs to a pair of jet events, with Monte Carlo truth information for event selection, the accuracy is three times better, as shown in Table 2. This superiority is due to better performance for track and jet reconstruction. On the other hand, the resolution for the $H \to \gamma\gamma$ events in APODIS is roughly 73% worse than in the LHC detectors. This is due to the fact that the LHC ECALs have a better intrinsic photon resolution than APODIS. Furthemore, the resolution of APODIS is also limited by the absence of geometry-based corrections and fine-tuned calibrations. Compared to the resolution (1.64%) when using a simplified geometry with the same ECAL geometry parameters [10], APODIS is still 58% worse.

Table 2. Benchmark resolutions (sigma/Mean) of reconstructed Higgs boson mass compared to the LHC results.

	$H \to \mu\mu$	$H \to \gamma\gamma$	$H \to bb$
CEPC (APODIS)	0.20%	2.59%[1]	3.63%
LHC (CMS, ATLAS)	~2% [25, 26]	~1.5% [27, 28]	~10% [29, 30]

[1] preliminary result without adequate geometry based corrections and fine-tuned calibrations.

In order to improve jet reconstruction performance, an event cleaning procedure has been developed. After event cleaning, the resolution of the reconstructed Higgs boson mass for different Higgs decay modes with jets as final state particles are comparable, as shown in Table 3.

Table 3. Higgs boson mass resolution (sigma/Mean) for different decay modes with jets as final state particles, after event cleaning.

$H \to bb$	$H \to cc$	$H \to gg$	$H \to WW^*$	$H \to ZZ^*$
3.63%	3.82%	3.75%	3.81%	3.74%

For $H \to WW^*$ and ZZ^* decay modes, the total invariant mass distribution is composed of multiple components depending on the decay modes of W and Z bosons. For the WW^* events, the classification is based on the leptonic or hadronic decay mode of W and W^* . For the ZZ^* events, the reconstruction result is sensitive to the visible or invisible decay mode of Z and Z^* . The distribution of $H \to ZZ^*$ is clearly separated with four peaks corresponding to the Z and Z^* decay modes. The standard cleaning procedure could efficiently veto the events with significant neutrinos generated from the Higgs boson cascade decay. After event cleaning, the Higgs boson mass resolution (sigma/Mean) for the $H \to WW^*$ and ZZ^* events is comparable with the Higgs to a pair of jet events, see Table 3.

We would like to thank Gang Li and Xin Mo for the physics event generator files.

References

1 ATLAS Collaboration, *Observation of a new particle in the search for the Standard Model Higgs boson with the ATLAS detector at the LHC*, Physics Letters B, **716**: 1-29 (2012), arXiv: 1207.7214 [hep-ex]
2 CMS Collaboration, S. Chatrchyan et al., *Observation of a new boson at a mass of 125 GeV with the CMS experiment at the LHC*, Physics Letters B **716**: 30-61 (2012), arXiv: 1207.7235 [hep-ex]
3 The CEPC-SPPC Study Group, *CEPC-SPPC Preliminary Conceptual Design Report*, http://cepc.ihep.ac.cn/preCDR/main_preCDR.pdf
4 Xinchou Lou, *Circular Electron-Positron Collider - Challenges and Opportunities*, presentation at IAS HEP conference, 2018, http://ias.ust.hk/program/shared_doc/2018/201801hep/conf/talks/HEP_20180123_0945_Xinchou_Lou.pdf
5 CMS Collaboration, *Projected Performance of an Upgraded CMS Detector at the LHC and HL-LHC: Contribution to the Snowmass Process*, CMS NOTE-13-002, arXiv: 1307.7135
6 ATLAS Collaboration, *Physics at a High-Luminosity LHC with ATLAS*, ATL-PHYS-PUB-2013-007, arXiv: 1307.7292
7 Zhen-Xing Chen et al., *Cross section and Higgs mass measurement with Higgsstrahlung at the CEPC*, Chinese Physics C, **41**(2): 023003 (2017), arXiv: 1601.05352
8 Manqi Ruan, *CEPC Baseline detector concept*, presentation at the Workshop on the CEPC-EU edition 2018, https://agenda.infn.it/getFile.py/access?contribId=23&sessiond=23&resId0&materiaId=slides&confId14816
9 M. Ruan, *Simulation, reconstruction and software at the CEPC*, presentation at CEPC workshop 2016, http://indico.ihep.ac.cn/event/5277/session/14/contribution/67/material/slides/0.pdf
10 H. Zhao et al, *Particle flow oriented electromagnetic calorimeter optimization for the circular electron positron collider*, Journal of Instrumentation, Volume 13, 2018, arXiv: 1712.09625
11 D. Yu, *Reconstruction of leptonic physic objects at future e+e- Higgs factory*, Ph.D Thesis, Paris Saclay, 2018, http://www.theses.fr/2018SACLX018
12 Manqi Ruan, *CEPC Detector design-optimization, Reconstruction and Performance*, presentation at IAS HEP conference 2018, http://ias.ust.hk/program/shared_doc/2018/201801hep/program/exp/HEP_20180119_1145_Manqi_Ruan.pdf
13 F. An et al, *Monte Carlo study of particle identification at the CEPC using TPC dE/dx information*, Eur. Phys. J. C, **78**: 464 (2018)
14 *CEPC software website*, http://cepcsoft.ihep.ac.cn/
15 W. Kilian et al, *Simulating Multi-Particle Processes at LHC and ILC*, Eur. Phys. J. C, **71**: 1742 (2011), arXiv: 0708.4233[hep-ph]
16 T. Sjöstrand, S. Mrenna, and P. Z. Skands, *PYTHIA 6.4 Physics and Manual*, JHEP, **0605**: 026 (2006), arXiv:hep-ph/0603175 [hep-ph]
17 P. Mora de Freitas and H. Videau, *Detector simulation with MOKKA/GEANT4: Present and future*, LC-TOOL-2003-010
18 Source code of MokkaPlus, http://cepcgit.ihep.ac.cn/cepcsoft/MokkaC
19 M. Ruan and H. Videau, *Arbor, a new approach of the Particle Flow Algorithm*, arxiv: 1403.4784[physics.ins-det]
20 M. Thomson, *Particle Flow Calorimetry and the PandoraPFA Algorithm*, Nucl.Instrum. Meth. A, **611**: 25, 40 (2009), arxiv: 0907.3577 [physics.ins-det]
21 C. Patrignani et al (Particle Data Group), *Review of Particle Physics*, Chinese Physics C, **40**: 100001 (2016)
22 M.Oreglia, *A study of the reactions* $\Psi' \to \gamma\gamma\Psi$, Ph.D. thesis, 1980
23 J. Gaiser, *Charmonium spectroscopy from radiative decays of the* J/Ψ *and* Ψ', Ph.D. thesis,1982
24 CMS collaboration, *Performance of photon reconstruction and identification with the CMS detector in proton-proton collisions at* $\sqrt{s}$ *= 8TeV*, JINST, **10**: P08010 (2015), arXiv: 1502.02702
25 CMS Collaboration, *Search for the standard model Higgs boson in the dimuon decay channel in pp collisions at sqrt(s)= 7 and 8 TeV*, CMS-PAS-HIG-13-007, http://cds.cern.ch/record/1606831
26 ATLAS Collaboration, *Letter of Intent for the Phase-II Upgrade of the ATLAS Experiment*, CERN-LHCC-2012-022, LHCC-I-023, https://cds.cern.ch/record/1502664/files/LHCC-I-023.pdf
27 CMS Collaboration, *Measurements of Higgs boson properties in the diphoton decay channel in proton-proton collisions at* $\sqrt{s}$ *= 13 TeV*, CMS-HIG-16-040, CERN-EP-2018-060, arXiv: 1804.02716
28 ATLAS Collaboration, *Measurements of Higgs boson properties in the diphoton decay channel with 36 fb*1 *of pp collision data at* $\sqrt{s}$ *=13 TeV with the ATLAS detector*, CERN-EP-2017-288, arXiv: 1802.04146
29 ATLAS Collaboration, *Evidence for the* $H \to b\bar{b}$ *decay with the ATLAS detector*, CERN-EP-2017-175, JHEP, **12**: 024 (2017), arXiv: 1708.03299
30 CMS collaboration (Evidence for the Higgs boson decay to a bottom quark-antiquark pair), Physics Letters B, **780**: 501-532 (2018)